Strange metal and coherence-incoherence crossover in pressurized $La_3Ni_2O_7$

L. Craco[1,2] and S. Leoni[3]

[1]*Institute of Physics, Federal University of Mato Grosso, 78060-900 Cuiabá, Mato Grosso, Brazil*
[2]*Leibniz Institute for Solid State and Materials Research Dresden, D-01069 Dresden, Germany*
[3]*School of Chemistry, Cardiff University, Cardiff CF10 3AT, United Kingdom*

(Received 4 October 2023; revised 20 March 2024; accepted 22 March 2024; published 5 April 2024)

The layered perovskite $La_3Ni_2O_7$ has attracted a great deal of attention recently due to the observation of unconventional superconductivity ($T_c \approx 80$ K) at high pressures. Motivated thereby, we present a computational study based on density functional plus dynamical mean-field theory calculations for the normal-state electronic reconstruction of a pressurized $La_3Ni_2O_7$ superconductor. We show how a coherence-incoherence crossover behavior manifests itself due to sizable electron correlation effects in the e_g-shell one-particle spectral functions. Our results capture the T dependence of the resistance, providing a many-particle interpretation for the emergent strange metal behavior seen in experiment. Our findings call for more studies on unconventional high-temperature superconductors to unearth the consequences of proximity to marginal Fermi liquidness as the prominent candidate in governing the transport anomalies of a strange metal.

DOI: 10.1103/PhysRevB.109.165116

I. INTRODUCTION

The normal state of a variety of correlated electron systems often falls into the strange metal category [1], where the electrical resistivity varies linearly with temperature [$\rho(T) = \rho_0 + AT$] as $T \to 0$ [2]. This generic property together with other experimental evidences, like the absence of the Drude peak in optics, incoherently broad line shape in spectroscopy, and strongly T-dependent Hall effects, represent significant deviations from the conventional Fermi liquid (FL) picture of good metals. Although the fundamental origin for this anomalous non-FL behavior [3] is under debate [4], the T-linear resistivity is often associated with quantum criticality [5]. On general grounds the strange metal phase exhibits a nonsaturating, T-linear resistivity that extends well beyond the Mott-Ioffe-Regel limit [6] at higher temperatures, due to vanishing quasiparticle excitations [7]. Examples of materials showing strange metal features or the absence of electron quasiparticles include Cu oxide [2] and heavy fermion materials at or close to a quantum critical point [3]. Remarkably as well within the strongly correlated strange metal context is the T-linear resistivity seen in magic-angle twisted bilayer graphene [8] as well as in $FeSe_{1-x}S_x$ sytems at high pressures [9]. Noteworthy is the recent discovery of unconventional high-temperature (high-T_c) superconductivity (SC) with critical temperature $T_c \approx 80$ K in the Ruddlesden-Popper bilayer perovskite nickelate $La_3Ni_2O_7$ under high pressures [10], also showing strange metal, T-linear resistivity in the normal state [10–12].

The discovery of high-T_c SC in Sr-doped $NdNiO_2$ films (T_c of 15 K) [13] has marked the nickel age of unconventional SC [14], putting the Ni-based superconductors rapidly into the newest branch of superconducting materials, following the cuprates [15] and Fe-based SCs [16]. In $La_3Ni_2O_7$, NiO_2 layers are, in fact, isostructural with CuO_2 layers in the cuprates. In the Ruddlesden-Popper $La_3Ni_2O_7$ bilayer nickelate [17], each unit cell consists of two NiO_2 layers connected by the Ni-O-Ni bond [18] through the oxygen p orbitals on the intercalating LaO layer. Under pressure, the $La_3Ni_2O_7$ experiences a structural phase transition during which the bonding angle increases from 168° to 180° along the c axis, [10] changing the orthorhombic space group from *Amam* to *Fmmm*, which in turn induces an insulator-metal transition [19] from weakly insulating [10,18,20] to metallic [10–12], under which SC emerges at high pressures. Unlike the infinite-layer nickelates with a Ni^{1+} nominal state ($3d^9$ electron configuration), a valence count gives $Ni^{2.5+}$ in the $La_3Ni_2O_7$ parent compound, corresponding to the $3d^{7.5}$ valence state [21]. As for $3d^6$ Fe-based SCs and the infinite-layer nickelates, this 7.5 total electron band filling gives rise to an interplay between multiband, multiorbital degrees of freedom and electron correlations [22–29] in determining the normal state, from which unconventional SC arises.

Existing first-principles density functional theory (DFT) calculations [10,23,26,29,30] show that the bands near the Fermi level (E_F) have mainly Ni-e_g orbital character, and bands with t_{2g} orbital character are located about 1.0 eV below E_F. They also reveal a sizable interlayer hopping between the Ni z^2 orbital through the apical oxygen, forming bonding-antibonding molecular states [23,25,30], characteristic of bilayer systems [31]. Based on earlier DFT studies and consistent with the ion valence count, the electronic state of each Ni ion in the unit cell consists of almost fully occupied t_{2g} and partially filled (1.5 electrons) e_g orbitals [21]. Inspired by earlier proposals [25,26], in this work we perform a two-orbital DFT plus dynamical mean-field theory (DFT + DMFT) [32] study, showing the emergent low-energy electronic structure reconstruction that underlies the strange metal normal state [10–12], which might host unconventional high-T_c SC in pressurized $La_3Ni_2O_7$.

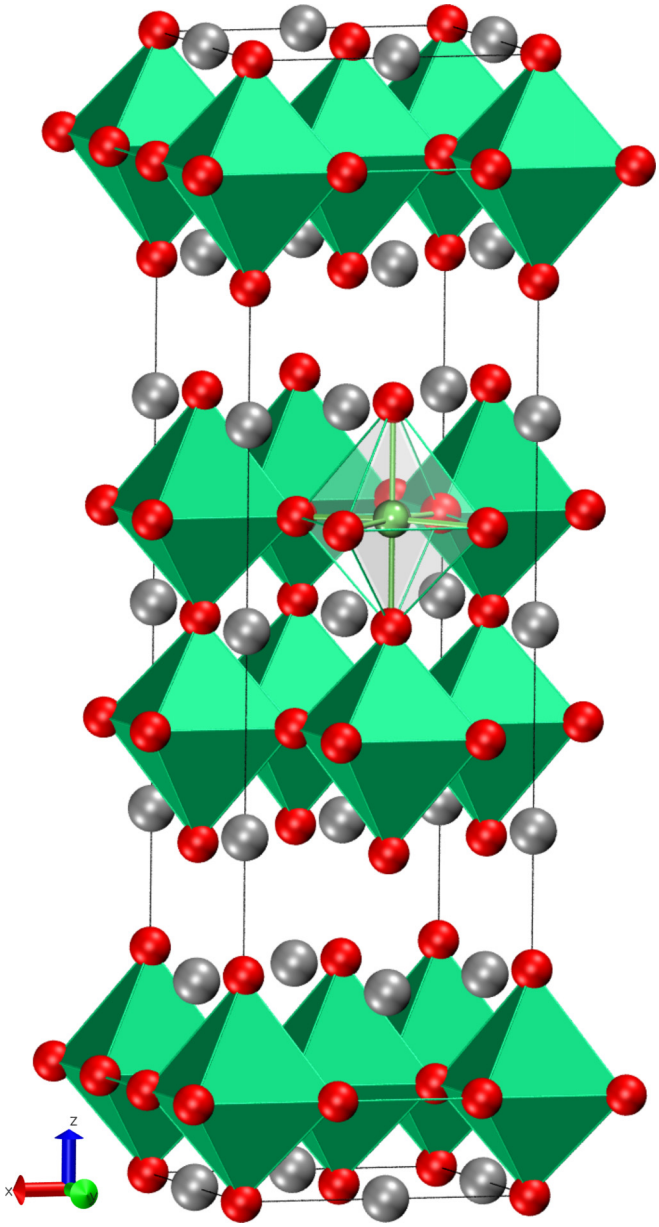

FIG. 1. High-pressure (25.0 GPa) *Fmmm* crystal structure of $La_3Ni_2O_7$ superconductor: Ni (green), La (gray), and O (red). The octahedral Ni coordination by O is highlighted within a bilayer.

II. THEORY AND RESULTS

Similar to infinite-layer nickelate superconductors [33–35], it has been recognized that the electronic properties of $La_3Ni_2O_7$ are determined by the complex interplay between different factors, including the on-site Coulomb repulsion ($2.04 \leqslant U \leqslant 10.0$ eV) [25–27,29,30], the Hund's interaction ($0.75 \leqslant J_H \leqslant 1.0$ eV) [27,29,34], and multiband and multiorbital (MO) degrees of freedom [23,24,27–29,35]. Based on DFT calculations [22,25,26] for the *Fmmm* structural phase (see Fig. 1), the two-orbital one-electron Hamiltonian pertinent to pressurized $La_3Ni_2O_7$ and analogs [36] is $H_0 = \sum_{\mathbf{k},a,\sigma} \epsilon_a(\mathbf{k}) c^\dagger_{\mathbf{k},a,\sigma} c_{\mathbf{k},a,\sigma}$, where $a = x^2 - y^2, z^2$ denotes its e_g orbitals and $\epsilon_a(\mathbf{k})$ is the corresponding band dispersion, which encodes details of the one-electron band structure [22]. These e_g orbitals are the one-particle inputs for two-orbital DMFT [25,26,34], which generates a coherent-incoherent crossover when approaching a marginal Fermi liquid (mFL) like the electronic state [37], as shown below. Neglecting the fully occupied Ni t_{2g} states at one-particle level [25,26], the correlated, two-orbital many-body Hamiltonian relevant to $La_3Ni_2O_7$ and analogs [34] reads $H_{\rm int} = U \sum_{i,a} n_{i,a,\uparrow} n_{i,a,\downarrow} + U' \sum_{i,a\neq b} n_{i,a} n_{i,b} - J_H \sum_{i,a\neq b} \mathbf{S}_{i,a} \cdot \mathbf{S}_{i,b}$. Here, $U' = U - 2J_H$ is the interorbital Coulomb interaction term. Given the complexity of the MO problem, with diagonal and off-diagonal lattice Green's functions and self-energies [38], here we work in the basis that diagonalizes the one-particle density matrix. In this basis, interorbital one-electron overlap is zero, and so in the paramagnetic phase we have $G_{a,b,\sigma}(\omega) = \delta_{a,b} G_{a,\sigma}(\omega)$ [39]. In this regime electrons among different orbitals interact only via the interorbital Coulomb interaction and the Hund's coupling. We evaluate the many-particle Green's functions $[G_{a,\sigma}(\omega)]$ of the two-orbital Hamiltonian $H = H_0 + H_{\rm int}$ using the two-orbital iterated perturbation theory as the impurity solver [40]. This real frequency perturbative *ansatz* has a proven record of good semiquantitative agreement with experiment for a range of correlated materials, including the infinite-layered $NdNiO_2$ superconductor [34], and it gives results in qualitative accord with continuous-time quantum Monte Carlo calculations for correlated multiorbital systems [41].

The IPT is an interpolative *ansatz* that connects the two exactly soluble limits of the one-band Hubbard model [42], namely, the uncorrelated ($U = 0$) and the atomic [$\varepsilon(\mathbf{k}) = 0$] limits. It accounts for the correct low- and high-energy behavior of the one-particle spectra and the metallic FL behavior in the large-D limit (DMFT) [43]. It ensures the Mott-Hubbard metal-insulator transition from a correlated FL metal to a Mott-Hubbard insulator as a function of the Coulomb interaction U. As shown below, the DFT + DMFT (MO-IPT) solution for $La_3Ni_2O_7$ introduces nontrivial effects stemming from the dynamical nature of strong electronic correlations. These processes lead to transfer of spectral weight across large energy scales in response to changes in the on-site Coulomb repulsion, a characteristic lying at the heart of the anomalous responses of correlated electron systems. We recall that a perturbative scheme similar to that used here for the two-orbital Hamiltonian of $La_3Ni_2O_7$ has been proposed in Ref. [44], where electron correlation effects in local-orbital electronic structure calculations were applied to Si bulk crystals and H_2O molecules. It is also worth noting that direct comparisons between MO-IPT results with numerically exact methods, like the continuous-time quantum Monte Carlo (CT-QMC), have been performed in recent years [45], showing only qualitative agreement between the two impurity solvers away from half-filling. However, in view of our previous studies on correlated electron systems showing good theory-experiment agreement [39,41], we are confident to use MO-IPT to explore the normal-state electronic structure reconstruction of the $La_3Ni_2O_7$ superconductor.

Bloch electronic states were calculated based on DFT in the Perdew-Burke-Ernzerhof (PBE) approximation, using Vanderbilt ultrasoft standard solid-state pseudopotentials. The

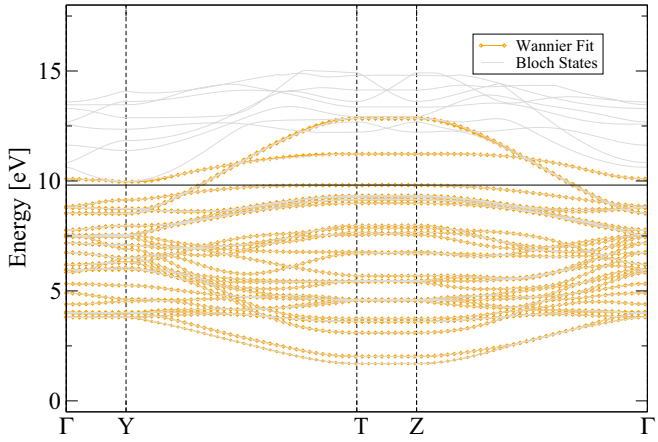

FIG. 2. Comparison between band structure (Bloch states, gray lines) and MLWF WANNIER fit (orange lines and orange diamonds) based on a 31-projector model (10 Ni $3d$ and 21 O $2p$ orbitals). The Fermi level is at $E = 9.8118$ eV.

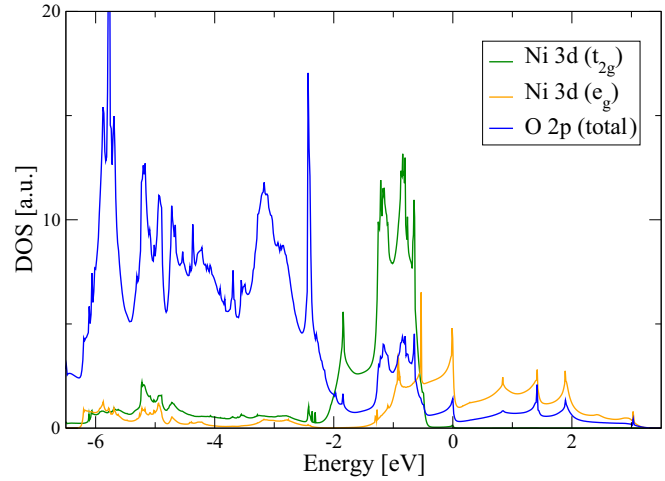

FIG. 3. Density of states (DOS) of Ni $3d$ e_g and t_{2g} states, together with total O $2p$ states, The contribution of O $2p$ at the Fermi level (shifted to 0 eV) is small compared to e_g states. At lower energies around -1 eV strong hybridization between Ni $3d$ t_{2g} is observed, due to Ni-O covalent bonds.

plane-wave expansion of valence electron wave functions and charge density used kinetic energy cutoffs of 90 and 850 Ry, respectively. Calculations were performed with the PW.X code (v7.0) of the QUANTUM ESPRESSO (QE) package. Wyckoff positions and lattice parameters were optimized at 25.0 GPa, starting from experimentally refined lattice parameters [10]. SCF calculations were run on a k-grid of $8 \times 8 \times 8$ data points. This yielded an optimized unit cell of 5.3260, 5.3261, and 20.5490 Å in the orthorhombic space group *Fmmm*. The corresponding Wyckoff positions (after transformation from the primitive QE setting) were Ni ($8i$), $z = 0.094\,896$; La ($8i$), $z = 0.320\,745$; O ($8i$), $z = 0.199\,835$; and O ($16j$) ,$z = 0.093\,239$. La ($4b$) and O ($4a$) are special positions without degrees of freedom.

A tight-binding band structure model was obtained from interpolating MLWFs, calculated with the WANNIER90 package [46] (v3.1). As an initial guess for Wannier functions (WF), $3d$ orbitals were used for Ni (10 MLWFs in total in the primitive cell). Valence O states were also included. Iterative spread minimization provided real-valued, maximally localized WF. Thirty-three Bloch states were considered after exclusion of lower-lying and empty states. An inner, frozen energy window in the range 1.5–9.97 eV was used to disentangle 10 Ni + 21 O states for wannierization (Fermi energy: 9.8118 eV). This choice guaranteed Ni localized, atomiclike WF, with the correct site symmetry and intersite symmetry equivalence. The resulting DFT orbital-resolved e_g density of states (DOS) of the high-pressure *Fmmm* phase (space group No. 69) [23] in Fig. 4 shows bare DOS similar to those reported in Ref. [22]. A comparison of Bloch states (bands) with the obtained WANNIER model is shown in Fig. 2. The DOS contribution of O $2p$ states at the Fermi level is low compared to that of Ni $3d$ e_g states (see Fig. 3).

As seen in Fig. 4, both the z^2 and the $x^2 - y^2$ orbitals are characterized by a particle-hole asymmetric electronic spectra, with clear van Hove singularities at different energies, a characteristic akin to low two-dimensional-like systems [43]. Interesting as well is the emergence of a van Hove singular peak in the z^2 channel at E_F, followed by an antibonding conduction band structure due to the Ni-O overlapping along the c direction [18]. The van Hove singularity located at the upper edge of the bonding band [22,30] and the narrow bandwidth of the z^2 orbital as compared to the planar $x^2 - z^2$ orbital imply stronger electron-electron interactions in the former.

Let us now present our DFT + DMFT results. In Fig. 4 we show how the orbital-resolved Ni e_g spectral functions of pressurized $La_3Ni_2O_7$ computed using three different U values and fixed $J_H = 0.75$ eV are reshaped as compared to the bare DFT DOS. As seen, at finite U the shape of the $x^2 - y^2, z^2$ spectra is partially shifted towards E_F due to correlation induced dynamical transfer of spectral weight. However, in good qualitative accord with earlier calculations, [25,26,29] lower (LHB) and upper (UHB) Hubbard bands emerge at high energies in the correlated electronic structure of pressurized $La_3Ni_2O_7$. Similar to $NdNiO_2$ [34], with increasing the on-site U, the spectral weights of these incoherent, Hubbard band electronic states are enhanced with the concomitant narrowing of the Kondo-quasiparticle resonances [43] at low energies near E_F. To further confirm the correlated electronic structure reconstruction in the normal state of the $La_3Ni_2O_7$ superconductor, in the insets of Fig. 4 we show the frequency dependence of the self-energy [$\Sigma_a(\omega)$] imaginary (right panels) and real (left panels) parts, where the latter determines the quasiparticle mass enhancement [25,27,29]. From our results, it is visible that $\mathrm{Re}\,\Sigma_{z^2}(\omega)$ has larger slope values as compared to the $x^2 - y^2$ orbital, yielding larger electron mass enhancement [43] as shown below. Albeit with smaller damping, our DFT + DMFT results in Fig. 4 reveal a quadratic energy dependency in $\mathrm{Im}\,\Sigma_a(\omega)$ at low frequencies similar to that in Refs. [27,29].

It is worth noting here that the appearance of stronger electronic correlations in the z^2 orbital as compared to the $x^2 - y^2$ orbital results from the interplay between the van Hove singularity located at E_F and the U/W (correlation to bare bandwidth) ratio. In low-dimensional systems the DOS usually diverges and the excess of charge carriers en-

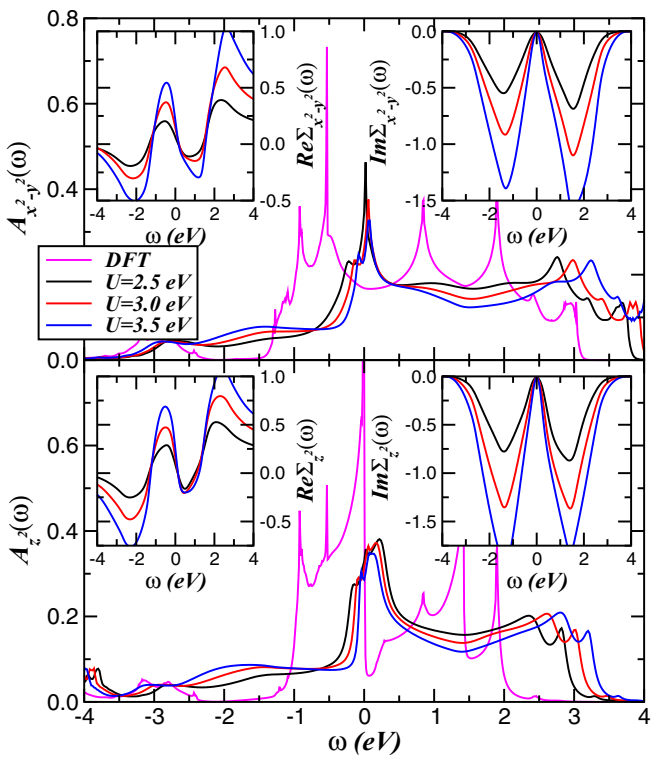

FIG. 4. Evolution of the e_g spectral functions of pressurized $La_3Ni_2O_7$ for three different U values and fixed $J_H = 0.75$ eV. The bare (DFT) DOS is shown for comparison. Notice the electronic reconstruction due to sizable two-orbital correlations and the formation of narrow Kondo-quasiparticles at low-energies near the Fermi level. Insets show the changes of the self-energy real (left panels) and imaginary (right panels) parts with increasing U. Here, all DFT + DMFT (MO-IPT) spectral functions are computed at zero temperature.

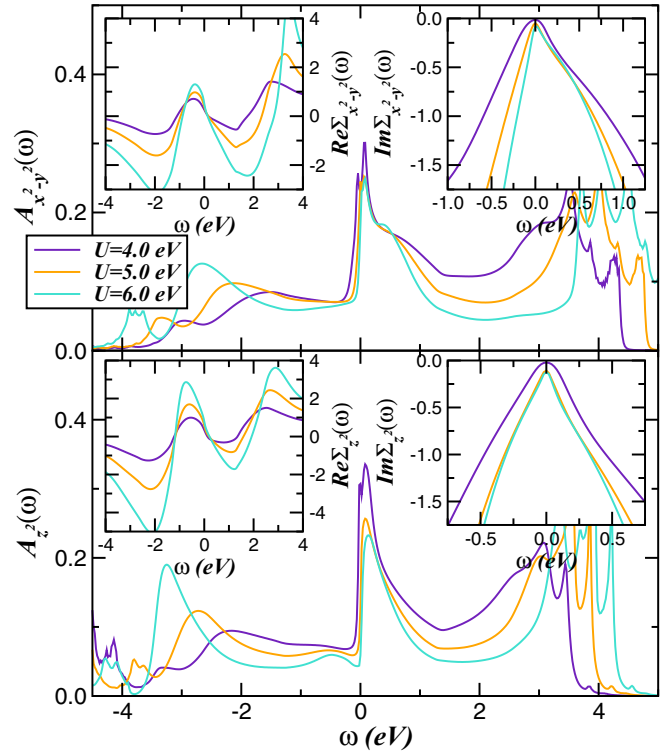

FIG. 5. Electronic reconstruction hidden in the coherence-incoherence crossover of a pressurized $La_3Ni_2O_7$ superconductor. Notice the loss of Fermi liquid coherence at low energies as well as the emergence of a pseudogapped z^2-orbital electronic state at $U \geqslant 5.0$ eV due to combined van Hove singularity and electron correlations effects. Insets display the frequency dependence of the self-energy imaginary and real parts, showing considerable changes with increasing U. The $\mathrm{Im}\Sigma_a(\omega)$ curves are plotted in a small energy window to visualize the correlation-induced damping in the normal state.

hances intrinsic electronic correlations [47], an effect which is commonly referred to as extended van Hove singularity [48]. It is interesting that, albeit orbital-selective, a similar effect also emerges in the electronic structure reconstruction of pressurized $La_3Ni_2O_7$. Thus, since the intensity of the bare DFT DOS at E_F is higher for the z^2 orbital compared to that of the $x^2 - y^2$ orbital, sizable intra- and interorbital Coulomb correlation effects induced by U and U' promote an extended van Hove singularity regime similar to that discussed, for example, for doped graphene [48] and Sr_2RuO_4 [49]. Finally, also relevant to the emergent correlated electronic state is the fact that the z^2 orbital is closer to half-filling as compared to the $x^2 - y^2$ orbital [26]. Taken together, these combined effects are the key step which allows one to understand the two-orbital electronic reconstruction in $La_3Ni_2O_7$ under high pressure conditions.

To unveil the strange metal seen in electrical transport experiments [10–12] of $La_3Ni_2O_7$, in Fig. 5 we show the changes in the orbital-resolved DOS upon further increasing the on-site Coulomb interaction U. Our results for U between 4.0 and 6.0 eV [23,27,29,30] in Fig. 5 reveal that the maxima of the DFT + DMFT DOS near E_F is reduced due to orbital-selective damping of the self-energy imaginary part [27], responsible for the coherence-incoherence crossover at low energies. Taken together, the DFT + DMFT electronic structure in Fig. 5 shows large-scale changes in spectral weight transfer when approaching the mFL electronic state. As shown in Fig. 5, the relative large range of damping of the emergent pseudoquasiparticles [50] is closely related to the frequency dependence of the self-energy imaginary parts, which apart from finite damping [$\mathrm{Im}\Sigma(0) \neq 0$] [27,29] show deviations from the ω^2 dependence of canonical FL metals [43] for $5.0 \leqslant U \leqslant 6.0$ eV. In this regime, the self-energies of the strongly interacting e_g fermions display sublinear (V-shaped-like) ω dependence also seen in power-law liquids [51]. Self-energy behavior similar to that in Fig. 5, with sublinear energy dependence, was also found in Fe-based superconductors [52], suggesting a common scenario for the MO electronic reconstruction in correlated SC materials. We shall mention here that internal thermalization, which usually comes from scatterings due to impurities or residual electron-lattice interactions, naturally induces electron incoherence due to finite self-energy imaginary parts. Thus, our results in Fig. 5 underline the importance of combined extended van Hove singularity and local dynamical correlations, and holds promise for understanding similar physics in correlated systems where thermalization may occur without temperature [53].

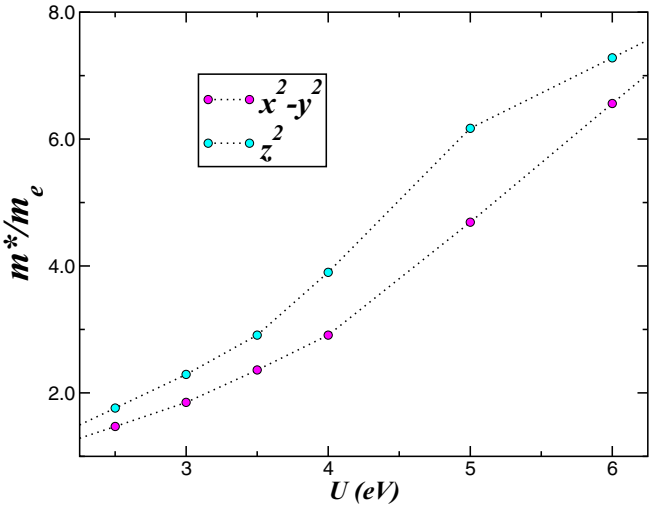

FIG. 6. e_g-orbital-resolved mass renormalization of pressurized $La_3Ni_2O_7$ superconductor as a function of the on-site U.

For the sake of completeness, we recall here the work by Varma *et al.* [37], where a mFL theory for the cuprate oxide superconductors was introduced. Aiming for a phenomenological explanation of strong deviations from a conventional FL metal, including the T-linear resistivity of the strange-metal phase [1,41], Varma *et al.* [37] proposed a momentum-independent one-particle self-energy arising from charge and spin fluctuations of the form $\Sigma_{mFL}(\omega, T) \sim g^2\rho^2(0)[\omega \ln \frac{x}{\omega_c} - i\frac{\pi}{2}x]$, where g is a coupling constant, $\rho(0)$ is the bare one-particle DOS at zero frequency, $x = \max(|\omega|, T)$, and ω_c is an ultraviolet cutoff. This phenomenological approach assumes that the energy-dependent local self-energy of cuprate oxides behaves like $\mathrm{Re}\Sigma_{\mathrm{mFL}}(\omega) \sim \omega \ln|\omega|$ and $\mathrm{Im}\Sigma_{mFL}(\omega) \sim -|\omega|$ in contrast to normal FL metals where $\mathrm{Re}\Sigma_{FL}(\omega) \sim -\omega$ and $\mathrm{Im}\Sigma_{FL}(\omega) \sim -\omega^2$ hold true at low energies [43]. Note that at zero T the mFL form of the self-energy implies the absence of electron quasiparticles [54] and linear ω dependence of $\mathrm{Im}\Sigma(\omega)$ near E_F. Similar to the hidden FL theory [50,55], the mFL theory has been shown to account for much of the transport anomalies in the layered cuprate oxides superconductors [37], although the microscopic origin of the strange metal remains largely unknown [56].

Since in DMFT the self-energy is momentum independent [43], the quasiparticle residue Z_a of an orbital a, which defines the renormalized Fermi energy, directly yields the effective electron mass enhancement: $\frac{m^\star_a}{m_e} = \frac{1}{Z_a} = (1 - \frac{\partial \mathrm{Re}\Sigma_a(\omega)}{\partial\omega})_{\omega=0}$, where m_e is the free electron mass. Thus, from the slope of the self-energy real part for $n = 1.5$ we have computed $\frac{m^\star_{z^2}}{m_e}$ and $\frac{m^\star_{x^2-y^2}}{m_e}$ of pressurized $La_3Ni_2O_7$. In Fig. 6 we display the U dependence of $\frac{m^\star}{m_e}$, showing results which are consistent with earlier DFT + DMFT studies [25,29]. On the other hand, our results away from the weakly correlated FL regime, i.e., $U > 3.0$ eV, are considerably larger as compared to the electron effective mass $m^*/m_e \approx 2.12$ inferred from specific heat measurements [57]. It is worth noting that we only observe effective electron mass enhancements consistent with existing observations in the FL regime. This suggests that different experiments might probe unequal degrees of multiband, MO correlations with competing orders [57].

Strange metallicity with clear deviation from the FL T dependence of the resistivity in the normal state above 70 K in experiment [11], as shown below, may provide additional support to our orbital-selective electronic structure of the $La_3Ni_2O_7$ superconductor. Specifically, we study the T dependence of the dc resistivity and correlate it with the orbital-reconstruction scenario derived above. Given the correlated spectral functions $A_a(\mathbf{k}, \omega) = -\frac{1}{\pi}\mathrm{Im}G_a(\mathbf{k}, \omega)$, the (static) dc conductivity $[\sigma_{dc}(T)]$, computed within the DMFT formalism [58,59], can be expressed as $\sigma_{dc}(T) = \frac{2\pi e^2}{\hbar\mathcal{V}} v^2 \sum_a \int d\epsilon A_a^{(0)}(\epsilon) \int d\omega A_a^2(\epsilon, \omega)[-f'(\omega)]$. In this expression, $A_a^{(0)}(\epsilon)$ is the bare DFT DOS of the a orbitals (Fig. 4), $\mathcal{V}$ is the unit cell volume, and $f(\omega)$ is the Fermi function. As in Ref. [60] the approximation made here is to ignore the $\mathbf{k}$ dependence of electron's velocity, $v_{\mathbf{k},a}$. In this situation, following Urasaki and Saso [61], we approximate $v_{\mathbf{k},a}$ by a single average carrier velocity (v) for the e_g orbitals. In fact, Refs. [61,62] have shown that this assumption works well for numerical computations of $\sigma_{ac}(\omega)$ for Kondo insulators (FeSi and YbB_{12}), V_2O_3, and Fe-pnictide superconductors, supporting our approximation in $\sigma_{dc}(T)$ above. Importantly, this approximation has also been used to study thermoelectric transport properties of p and d band systems [63], showing good theory-experiment agreement in various cases. The observed features in resistivity $\rho_{dc}(T) \equiv 1/\sigma_{dc}(T)$ originate from correlation-induced spectral changes: Showing how this provides a compelling description of extant experimental data [11] is our focus here.

In Fig. 7 we display the T dependence of the electrical resistivity, $\rho(T) \equiv 1/\sigma_{dc}(T)$, computed using the $T = 0$ orbital-resolved DFT + DMFT spectral functions of compressed $La_3Ni_2O_7$ for fixed $J_H = 0.75$ eV and the three U values considered in Fig. 5. As seen in Fig. 7, the DFT + DMFT result for $La_3Ni_2O_7$ parent compound shows nearly T-linear resistivity, a fingerprint of the normal-state strange metal seen in experiment [10–12]. Clearly, since we do not consider the SC phase, the resistivity curves should only be trusted above T_c. While in experiment the resistance shows T-linear behavior above $T_c \approx 70$ K [11] at 26.6 GPa, our results in Fig. 7 are in good qualitative accord with those reported in Ref. [11] up to 160 K, where the theory result starts to deviate from experiment. Interestingly, upon increasing the on-site U, the intensity and the slope A of $\rho(T)$ show appreciable electron correlation dependence; however, no signs of saturation up to 300 K similar to that obtained within the hidden FL theory [55] are found in $\rho(T)$. Thus, consistent with Ref. [29], our correlated electron picture derived from DFT + DMFT might have important implications for understanding a major experimental observation in pressurized $La_3Ni_2O_7$, namely, its strange metallicity in the normal state. The linear-in-T resistivity arising in our picture is linked to the combined effect of orbital-dependent damping [27] with the V-shape-like ω dependence of the self-energy imaginary parts shown in Fig. 5. Here it may be tempting to consider the expression $[(\hbar\omega)^2 + (\beta k_B T)^2]^\gamma$ (the parameter β governs the comparative strengths of temperature and energy [64] and $\gamma = 1/2$ for the strange metal) [65], which gives a quasiparticle lifetime inversely proportional to both the frequency and the tempera-

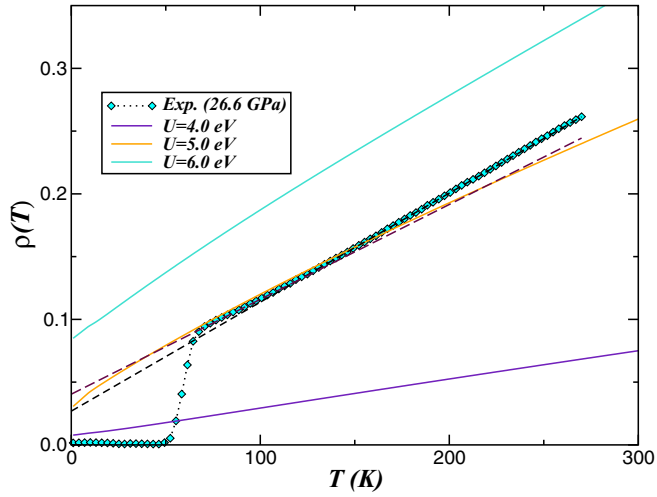

FIG. 7. Resistivity (resistance in experiment) versus temperature of $La_3Ni_2O_7$ superconductor obtained using the DFT + DMFT spectral functions for fixed total e_g occupancy $n = 1.5$ and three different U values. The theory curves are renormalized to the $U = 5.0$ eV to coincide with the experimental result at T around 150 K. Here, the resistivity curves are computed using the $T = 0$ orbital-resolved DFT + DMFT spectral functions (see Fig. 5) of compressed $La_3Ni_2O_7$. Notice the quasilinear T dependence of transport data in the normal state above 70 K in experiment [11], which is qualitatively reproduced by DFT + DMFT. Also noteworthy is the pronounced U dependence of resistivity, which can be controlled in experiment by tuning the correlation to bandwidth ratio.

ture. [29] The latter is often used as an indicator of Planckian dissipation arising from strange metallicity in the normal state [65,66]. Thus, motivated by the phenomenological form for the electronic scattering rate of power law liquids (PLL) of Ref. [64], $\mathrm{Im}\Sigma_{PLL}(\omega) = \Gamma_0 + \eta[(\hbar\omega)^2 + (\beta k_B T)^2]^{\gamma}$, as well as the difficulty in constructing a microscopic theory for the strange metal [1,55,56], based on our study we propose that the Planckian dissipation time τ_P [65] can be expressed in terms of the self-energy imaginary part at E_F, i.e., $\tau_P = \frac{\hbar}{|Im\Sigma(\omega,T)|_{\omega=0}}$. Being a correlated many-particle generalization of Plank's relation $\tau_P = \frac{\hbar}{k_B T}$ [65,66], this equation shall microscopically describe among other physical quantities [67] the shortest time for both energy and heat [65] loss in a quantum many-body system.

III. CONCLUSION

To summarize, we have used DFT + DMFT for a two-orbital Hubbard model to derive a correlation-induced electronic structure reconstruction of pressurized $La_3Ni_2O_7$ superconductor. In particular, considering $La_3Ni_2O_7$ as a suitable template, we have analyzed its normal-state strange metal behavior, unraveling it as an interplay between self-energy damping and its proximity to a marginal Fermi liquid metal, both arising from a combined extended van Hove singularity and two-orbital dynamical correlations. Our work provides a motivation to consider closer similarities between compressed $La_3Ni_2O_7$ and other strange metal candidates [65], where superconductivity manifests as an instability of an anomalous metal [1]. Based on a theory-experiment comparison we suggest that $La_3Ni_2O_7$ is a candidate for testing this and the idea of correlation-induced coherence-incoherence crossover and the emergence of damped pseudo-quasiparticles at low temperatures.

ACKNOWLEDGMENTS

Acknowledgment (L.C.) is made to CNPq and CAPES as well as to J. Fink for helpful comments and useful discussions. S.L. thanks the Leverhulme Trust for support under Project No. RPG-2020-052 and ARCCA Cardiff for computational support.

[1] P. W. Anderson, Nat. Phys. **2**, 626 (2006).
[2] A. Legros *et al.*, Nat. Phys. **15**, 142 (2019); see also J. Wu and I. Bozovic, Sci. Bull. **68**, 851 (2023).
[3] G. R. Stewart, Rev. Mod. Phys. **73**, 797 (2001).
[4] T. Andrade, A. Krikun, K. Schalm, and J. Zaanen, Nat. Phys. **14**, 1049 (2018).
[5] E. Abrahams and Q. Si, J. Phys.: Condens. Matter **23**, 223201 (2011); J. A. N. Bruin, H. Sakai, R. S. Perry, and A. P. Mackenzie, Science **339**, 804 (2013); J. Vučičević, D. Tanasković, M. J. Rozenberg, and V. Dobrosavljević, Phys. Rev. Lett. **114**, 246402 (2015); J. Wang, Y.-Y. Chang, C.-Y. Mou, S. Kirchner, and C.-H. Chung, Phys. Rev. B **102**, 115133 (2020).
[6] J. Merino and R. H. McKenzie, Phys. Rev. B **61**, 7996 (2000); see also T. Hu, Y. Liu, H. Xiao, G. Mu, and Y.-f. Yang, Sci. Rep. **7**, 9469 (2017), and references therein.
[7] M. Blake, R. A. Davison, and S. Sachdev, Phys. Rev. D **96**, 106008 (2017).
[8] Y. Cao, D. Chowdhury, D. Rodan-Legrain, O. Rubies-Bigorda, K. Watanabe, T. Taniguchi, T. Senthil, and P. Jarillo-Herrero, Phys. Rev. Lett. **124**, 076801 (2020); H. Polshyn, M. Yankowitz, S. Chen, Y. Zhang, K. Watanabe, T. Taniguchi, C. R. Dean, and A. F. Young, Nat. Phys. **15**, 1011 (2019).
[9] H. Okabe, N. Takeshita, K. Horigane, T. Muranaka, and J. Akimitsu, Phys. Rev. B **81**, 205119 (2010); J. P. Sun *et al.*, Nat. Commun. **7**, 12146 (2016); Phys. Rev. Lett. **118**, 147004 (2017); K. Matsuura *et al.*, Nat. Commun. **8**, 1143 (2017).
[10] H. Sun *et al.*, Nature (London) **621**, 493 (2023).
[11] Y. Zhang *et al.*, arXiv:2307.14819.
[12] G. Wang, N. N. Wang, X. L. Shen, J. Hou, L. Ma, L. F. Shi, Z. A. Ren, Y. D. Gu, H. M. Ma, P. T. Yang *et al.*, Phys. Rev. X **14**, 011040 (2024).
[13] D. Li, K. Lee, B. Y. Wang, M. Osada, S. Crossley, H. R. Lee, Y. Cui, Y. Hikita, and H. Y. Hwang, Nature (London) **572**, 624 (2019).
[14] Y. Ji, J. Liu, L. Li, and Z. Liao, J. Appl. Phys. **130**, 060901 (2021); X. Zhou *et al.*, Mater. Today **55**, 170 (2022).
[15] J. G. Bednorz and K. A. Müller, Z. Phys. B **64**, 189 (1986).
[16] Y. Kamihara, T. Watanabe, M. Hirano, and H. Hosono, J. Am. Chem. Soc. **130**, 3296 (2008).

[17] F. Gervais, P. Odier, and Y. Nigara, Solid State Commun. **56**, 371 (1985).

[18] T. Hosoya, K. Igawa, Y. Takeuchi, K. Yoshida, T. Uryu, H. Hirabayashi, and H. Takahash, J. Phys.: Conf. Ser. **121**, 052013 (2008).

[19] V. Pardo and W. E. Pickett, Phys. Rev. B **83**, 245128 (2011).

[20] G. Wu, J. J. Neumeier, and M. F. Hundley, Phys. Rev. B **63**, 245120 (2001).

[21] H. LaBollita, V. Pardo, M. R. Norman, and A. S. Botana, arXiv:2309.17279.

[22] Z. Luo, X. Hu, M. Wang, W. Wú, and D.-X. Yao, Phys. Rev. Lett. **131**, 126001 (2023).

[23] Y. Zhang, L.-F. Lin, A. Moreo, and E. Dagotto, Phys. Rev. B **108**, L180510 (2023).

[24] Y. Shen, M. Qin, and G.-M. Zhang, Chin. Phys. Lett. **40**, 127401 (2023); Y.-B. Liu, J.-W. Mei, F. Ye, W.-Q. Chen, and F. Yang, Phys. Rev. Lett. **131**, 236002 (2023); H. Oh and Y.-H. Zhang, Phys. Rev. B **108**, 174511 (2023); see also H. Sakakibara, N. Kitamine, M. Ochi, and K. Kuroki, Phys. Rev. Lett. **132**, 106002 (2024); Y. Gu, C. Le, Z. Yang, X. Wu, and J. Hu, arXiv:2306.07275; C. Lu, Z. Pan, F. Yang, and C. Wu, arXiv:2307.14965; Y.-H. Tian, Y. Chen, J.-M. Wang, R.-Q. He, and Z.-Y. Lu, arXiv:2308.09698.

[25] F. Lechermann, J. Gondolf, S. Bötzel, and I. M. Eremin, Phys. Rev. B **108**, L201121 (2023).

[26] V. Christiansson, F. Petocchi, and P. Werner, Phys. Rev. Lett. **131**, 206501 (2023).

[27] D. A. Shilenko and I. V. Leonov, Phys. Rev. B **108**, 125105 (2023).

[28] W. Wú, Z. Luo, D.-X. Yao, and M. Weng, Sci. China Phys. Mech. Astron. **67**, 117402 (2024).

[29] Y. Cao and Y.-F. Yang, Phys. Rev. B **109**, L081105 (2024).

[30] Z. Liao, L. Chen, G. Duan, Y. Wang, C. Liu, R. Yu, and Q. Si, Phys. Rev. B **108**, 214522 (2023).

[31] N. Kitamine, M. Ochi, and K. Kuroki, Phys. Rev. Res. **2**, 042032(R) (2020); L. Craco, Eur. Phys. J. B **95**, 125 (2022).

[32] G. Kotliar, S. Y. Savrasov, K. Haule, V. S. Oudovenko, O. Parcollet, and C. A. Marianetti, Rev. Mod. Phys. **78**, 865 (2006).

[33] F. Lechermann, Phys. Rev. X **10**, 041002 (2020); P. Werner and S. Hoshino, Phys. Rev. B **101**, 041104(R) (2020); P. Adhikary, S. Bandyopadhyay, T. Das, I. Dasgupta, and T. Saha-Dasgupta, *ibid.* **102**, 100501(R) (2020); Y. Wang, C.-J. Kang, H. Miao, and G. Kotliar, *ibid.* **102**, 161118(R) (2020); S. Ryee, H. Yoon, T. J. Kim, M. Y. Jeong, and M. J. Han, *ibid.* **101**, 064513 (2020); E. Been, W. S. Lee, H. Y. Hwang, Y. Cui, J. Zaanen, T. Devereaux, B. Moritz, and C. Jia, Phys. Rev. X **11**, 011050 (2021); J. Karp, A. Hampel, and A. J. Millis, Phys. Rev. B **103**, 195101 (2021).

[34] L. Craco, A. S. de Arruda, and S. Leoni, Phys. Rev. Res. **4**, 043036 (2022).

[35] L. Craco and S. Leoni, Phys. Rev. Mater. **7**, 044802 (2023).

[36] H. Sakakibara *et al.*, arXiv:2309.09462.

[37] C. M. Varma, P. B. Littlewood, S. Schmitt-Rink, E. Abrahams, and A. E. Ruckenstein, Phys. Rev. Lett. **63**, 1996 (1989).

[38] See, for example, A. Koga, N. Kawakami, T. M. Rice, and M. Sigrist, Phys. Rev. B **72**, 045128 (2005).

[39] See, L. Craco, M. S. Laad, S. Leoni, and E. Müller-Hartmann, Phys. Rev. B **70**, 195116 (2004).

[40] L. Craco, Phys. Rev. B **77**, 125122 (2008).

[41] L. Craco and S. Leoni, Phys. Rev. B **100**, 121101(R) (2019).

[42] H. Kajueter and G. Kotliar, Phys. Rev. Lett. **77**, 131 (1996).

[43] A. Georges, G. Kotliar, W. Krauth, and M. J. Rozenberg, Rev. Mod. Phys. **68**, 13 (1996).

[44] P. Pou, R. Pérez, F. Flores, A. Levy Yeyati, A. Martin-Rodero, J. M. Blanco, F. J. García-Vidal, and J. Ortega, Phys. Rev. B **62**, 4309 (2000).

[45] See, for example, N. Dasari, W. R. Mondal, P. Zhang, J. Moreno, M. Jarrell, and N. S. Vidhyadhiraja, Eur. Phys. J. B **89**, 202 (2016); L.-F. Arsenault, P. Sémon, and A.-M. S. Tremblay, Phys. Rev. B **86**, 085133 (2012); see also R. Mizuno, M. Ochi, and K. Kuroki, **104**, 035160 (2021).

[46] G. Pizzi *et al.*, J. Phys.: Condens. Matter **32**, 165902 (2020).

[47] S. Link *et al.*, Phys. Rev. B **100**, 121407(R) (2019); P. Rosenzweig, H. Karakachian, D. Marchenko, K. Kuster, and U. Starke, Phys. Rev. Lett. **125**, 176403 (2020).

[48] J. L. McChesney, A. Bostwick, T. Ohta, T. Seyller, K. Horn, J. Gonzalez, and E. Rotenberg, Phys. Rev. Lett. **104**, 136803 (2010); see also L. Craco, Phys. Rev. B **103**, 075135 (2021), and references therein.

[49] A. Liebsch and A. Lichtenstein, Phys. Rev. Lett. **84**, 1591 (2000).

[50] P. W. Anderson, Phys. Rev. B **78**, 174505 (2008).

[51] P. A. Casey and P. W. Anderson, Phys. Rev. Lett. **106**, 097002 (2011); K. Limtragool, C. Setty, Z. Leong, and P. W. Phillips, Phys. Rev. B **94**, 235121 (2016); Z. Leong, C. Setty, K. Limtragool, and P. W. Phillips, *ibid.* **96**, 205101 (2017).

[52] See, for example, L. Craco and S. Leoni, Sci. Rep. **7**, 46439 (2017).

[53] D. J. Luitz, R. Moessner, S. L. Sondhi, and V. Khemani, Phys. Rev. X **10**, 021046 (2020).

[54] M. A. Sulangi and J. Zaanen, Phys. Rev. B **98**, 094518 (2018).

[55] P. W. Anderson and P. A. Casey, Phys. Rev. B **80**, 094508 (2009).

[56] J. K. Jain and P. W. Anderson, Proc. Natl. Acad. Sci. USA **106**, 9131 (2009); D. V. Else and T. Senthil, Phys. Rev. Lett. **127**, 086601 (2021); L. V. Delacrétaz, B. Goutéraux, and V. Ziogas, **128**, 141601 (2022).

[57] J. Koepsell *et al.*, Science **374**, 82 (2021); Z. Liu *et al.*, Sci. China: Phys., Mech. Astron. **66**, 217411 (2023).

[58] K. Haule and G. Kotliar, New J. Phys. **11**, 025021 (2009).

[59] C. Grenzebach, F. B. Anders, and G. Czycholl, Phys. Rev. B **74**, 195119 (2006).

[60] L. Craco and S. Leoni, Sci. Rep. **5**, 13772 (2015).

[61] K. Urasaki and T. Saso, J. Phys. Soc. Jpn. **68**, 3477 (1999); T. Saso, *ibid.* **73**, 2894 (2004).

[62] L. Baldassarre *et al.*, Phys. Rev. B **77**, 113107 (2008); M. S. Laad, L. Craco, S. Leoni, and H. Rosner, **79**, 024515 (2009).

[63] L. Craco and M. S. Laad, Eur. Phys. J. B **89**, 119 (2016); L. Craco, T. A. da Silva Pereira, and S. Leoni, Phys. Rev. B **96**, 075118 (2017); L. Craco and S. Leoni, APL Energy **2**, 016102 (2024).

[64] T. J. Reber *et al.*, Nat. Commun. **10**, 5737 (2019).

[65] P. W. Phillips, N. E. Hussey, and P. Abbamonte, Science **377**, eabh4273 (2022).

[66] S. A. Hartnoll and A. P. Mackenzie, Rev. Mod. Phys. **94**, 041002 (2022).

[67] C. Yang *et al.*, Nature (London) **601**, 205 (2022).